REVIEW ARTICLE | FOCUS
PUBLISHED ONLINE: 30 NOVEMBER 2010 | DOI: 10.1038/NPHOTON.2010.267
nature photonics

Nanoscale X-ray imaging

Anne Sakdinawat* and David Attwood

Recent years have seen significant progress in the field of soft- and hard-X-ray microscopy, both technically, through developments in source, optics and imaging methodologies, and also scientifically, through a wide range of applications. While an ever-growing community is pursuing the extensive applications of today's available X-ray tools, other groups are investigating improvements in techniques, including new optics, higher spatial resolutions, brighter compact sources and shorter-duration X-ray pulses. This Review covers recent work in the development of direct image-forming X-ray microscopy techniques and the relevant applications, including three-dimensional biological tomography, dynamical processes in magnetic nanostructures, chemical speciation studies, industrial applications related to solar cells and batteries, and studies of archaeological materials and historical works of art.

X-ray imaging at the nano- and microscale is of great interest for applications in the physical and life sciences. The associated wavelength range[1] extends from a few nanometres to a small fraction of a nanometre, offering the potential to image objects at this spatial resolution. The concomitant photon energies of such wavelengths extend from a few hundred electronvolts to several tens of kilo-electronvolts, spanning the spectroscopic features of essentially all elements and thereby providing a simple mechanism for identifying elements and probing chemical bonds by imaging with photon energies near an absorption edge. Furthermore, the large penetration depth of X-rays allows relatively thick samples to be imaged.

The early visionaries of X-ray microscopy saw the opportunity to extend microscopic imaging by utilizing the short wavelengths, elemental specificity and penetration depth of X-rays. They also saw the need to develop appropriate X-ray optics to realize this goal. Pioneering efforts were made by Kirkpatrick and Baez[2], who pursued the development of crossed reflective optics operating at glancing incidence, and Baez[3], who suggested the use of Fresnel zone plates. Reviews of the early history of X-ray imaging are given in several papers[4–9].

For soft X-rays, significant progress towards nanoscale imaging began in the 1970s and 1980s with the work of Schmahl and colleagues, who pursued the development of full-field transmission X-ray microscopy[10,11], and Kirz and colleagues, who investigated scanning transmission X-ray microscopy[12,13]. Both groups employed zone plate optics[14] (Fig. 1a) and synchrotron radiation. In this early work, the emphasis was on biological imaging in the 'water window' — between the absorption K-edges of carbon at 284 eV and oxygen at 543 eV — where water is relatively transparent and absorption by carbon-containing cellular sub-substructure provides a natural contrast mechanism. Spatial resolutions were around 100–200 nm in this early work, moving towards 50 nm in the late-1980s, and finally towards 10 nm today[15,16]. In addition to diffractive optics, normal-incidence reflective optics with multilayer coatings such as Schwarzschild optics[17] (Fig. 1b) were pursued by Cerrina *et al.*[18] in the 1980s, primarily for the scanning photoemission microscopy of material surfaces. Such optics have the advantages of a long working distance for photoemission studies, generally operating at photon energies of the order of 100 eV, and now being capable of achieving spatial resolutions down to tens of nanometres.

For harder X-rays — several to tens of kilo-electronvolts — early X-ray microscopy efforts were based largely on the use of curved reflective optics at near-glancing angles of incidence, at which the total external reflection of X-rays provides high reflectivity within the critical angle (typically between a fraction of a degree and several degrees[1]). An example that is still widely used today is the Kirkpatrick–Baez (KB) mirror pair (Fig. 1c), which consists of crossed curved mirrors focusing or imaging in orthogonal directions. More challenging optics such as a pair of matched axisymmetric conical sections (known as Wolter type I and II optics[19], after their inventor) have also been considered, and are indeed still used in X-ray astronomy, but suffer from considerable fabrication challenges, cost and limited collection solid angle. Resolutions using reflective optics from the 1950s to the 1980s were generally limited to a fraction of a micrometre[20] but have drastically improved to around 7 nm today[21]. In the 1990s, Snigirev *et al.* demonstrated that the refraction of hard X-rays was possible through the use of compound refractive lenses[22,23]. These lenses are not compatible with lower photon energies due to their high absorption, but are used at 10 keV or more for focusing, alignment and, more recently, for the imaging[24] of hard X-rays at synchrotron facilities. High-resolution Fresnel zone plates, originally seldom used with hard X-rays due to their low efficiencies, have become more commonplace in hard-X-ray microscopy[25] over the past decade as efficiency limitations have been overcome.

This Review provides a summary of the recent developments in X-ray optics and the current capabilities of direct image-forming X-ray microscopy techniques. X-ray diffractive and holographic microscopy techniques are reviewed in an accompanying article in this issue by Chapman and Nugent[26]. The use of X-ray microscopy is illustrated through its applications in materials science, biology, environmental sciences and cultural heritage performed at synchrotron facilities around the world. Recent progress in the development of compact X-ray microscopes is also highlighted, and finally the future outlook and challenges are discussed.

X-ray optics and technological progress

Advances in nanofabrication capabilities, electron beam lithography and thin-film deposition have allowed diffractive and reflective X-ray optics to be improved over time. The optics in an X-ray microscopy system are generally utilized either for focusing or as an image-forming objective. Zone plates are versatile high-resolution optics that are used for both image-formation and focusing with soft and hard X-rays. The spatial resolution in a zone-plate-based microscope is set largely by the outer zone width of the zone plate, assuming minimal aberrations, proper illumination and stable operation. The choice of zone plate parameters is typically set by the application: what photon energy is best for the sample under study, what resolution is desired (that is, the smallest achievable

Electrical Engineering and Computer Sciences, University of California at Berkeley, Berkeley, California 94720, USA. *e-mail: annesak@berkeley.edu

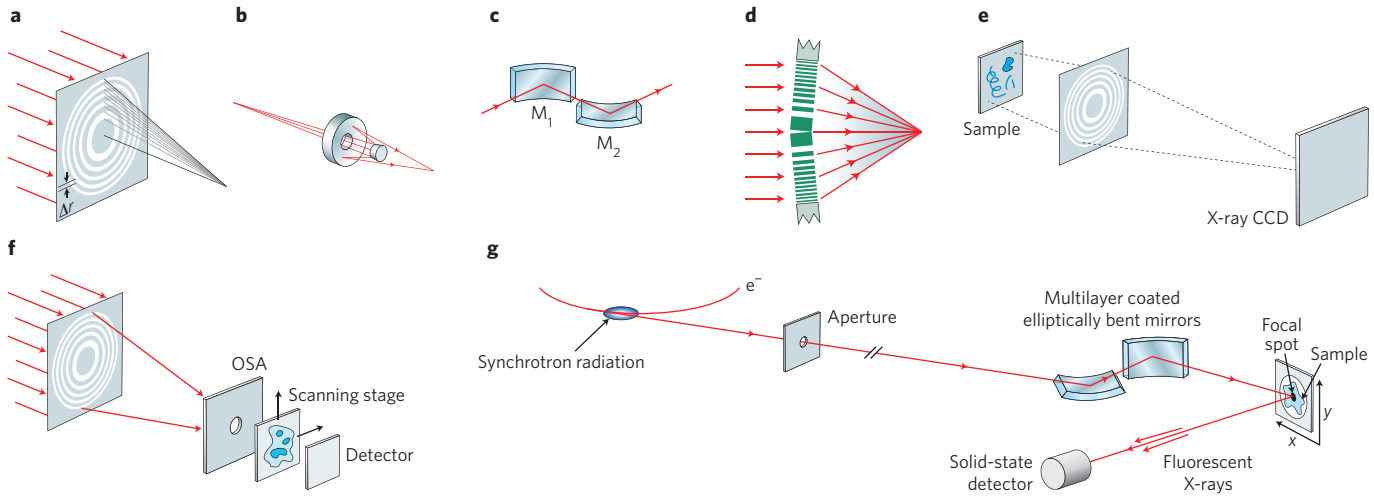

Figure 1 | Four common X-ray microscopy optics (a–d) and three common image-forming systems (e–g). a, A Fresnel zone plate lens is a circular diffractive structure that can be used for focusing or imaging X-rays, shown here as a focusing element. With spatially coherent illumination, the focal spot size is set by the outer zone width Δr, with a Rayleigh resolution of $1.2\Delta r$. **b**, A multilayer-coated two-bounce Schwarzschild reflective objective for focusing or imaging. The multilayer coating generally limits the efficiency to wavelengths greater than several nanometres. **c**, A KB glancing incidence mirror pair (M_1, M_2) for focusing hard X-rays. Multilayer coatings are sometimes used for photon energy selection and to increase the angles of operation. **d**, A multilayer Laue lens for focusing X-rays. This optic uses multilayer coatings to achieve thin, very high aspect ratio zones, of variable period, which are suitable for the nanoscale focusing of hard X-rays. **e**, Full-field TXM showing a back-illuminated sample, with transmitted photons imaged at high magnification to an X-ray-sensitive CCD array detector by a high-resolution zone plate. Limits on the angular illumination cone are used to control zero and higher order radiation. Illumination control is important for achieving maximum resolution. **f**, Zone-plate-based STXM showing X-rays focused to a small spot on a raster-scanned sample, with a detector recording transmitted photons as a function of scanning time. An order-sorting aperture (OSA) is used in conjunction with a thick central zone to block zero and higher order radiation[1]. **g**, Scanning μ-XRF microprobe based on a multilayer-coated KB mirror pair and bending magnet synchrotron radiation. Alternatively, operating in transmission mode with a high-spectral-resolution crystal monochromator and an upstream undulator as the source, the KB microprobe can be used for a variety of microscale X-ray absorption spectroscopy techniques such as μ-XANES. This system can also be used in transmission mode for μ-XRD. Figure reproduced with permission from: **a**–**c**,**e**–**g**, ref. 1, © 2000 Cambridge University Press; **d**, ref. 30, © 2008 AIP.

outer zone width, Δr) and what number of zones (N) should be used. The upper limit of N is set by the relative spectral bandwidth of the source. Deciding these three quantities automatically sets all other parameters such as diameter, focal length, numerical aperture and depth of focus (or field). Zone plates are fabricated using electron-beam lithography and electroplating/etching of a metal. Zone plates work on the basis of the interference of radiation from across the structure, which therefore requires an electron-beam placement accuracy of at least $\Delta r/3$. These structures must be sufficiently thick to provide suitable efficiency, primarily through the absorption of soft X-rays, but with an ever-stronger phase shifting component for harder X-rays. Zone plate efficiencies are typically around 10% in the first order, but vary depending on the choice of material, the duty cycle, substrate attenuation, and thickness and grading of the zones. Aspect ratios of only 3:1 or 4:1 are normal for the highest-resolution zone plates, which limits the diffraction efficiency, but recent progress has demonstrated structures with aspect ratios of greater than 20:1 for $\Delta r = 25$ (ref. 27). Several processing tricks can be used to obtain narrower but thicker structures, including zone plate stacking[28], zone doubling[15] through atomic layer deposition, and double patterning[29], a technique used widely throughout the semiconductor industry. Current expectations are that zone plate imaging will be extended to less than 10 nm, but its utility in scientific applications at that resolution will depend on the object contrast, radiation dose, depth-of-field and available working distance.

A different approach for improving the resolution and efficiency of hard-X-ray focusing is to use a multilayer Laue lens[30], which is essentially a one-dimensional (1D) zone plate based on multilayer coatings fabricated by magnetron sputtering, with varied d-spacing. These are coated, sectioned and polished to an equivalent outermost zone width as small as 4 nm, with several thousand zones and a thickness greater than 10 μm, thus providing an extremely high aspect ratio when used in the transmission geometry. Use of side-by-side multilayer Laue lenses in a tilted geometry (Fig. 1d) provides higher efficiency, resulting in 1D focusing to 16 nm at 20 keV (ref. 30). A second pair of such lenses used in the orthogonal direction will, in the future, provide full 2D focusing or imaging. Pursuit of imaging geometries that have higher aspect ratios and smaller outermost zone widths (that is, higher efficiencies and even better resolution) will require the use of tapered d-spacings and curved substrates[31].

Reflective optics are used for focusing in the field of hard-X-ray imaging and are expected to achieve imaging resolutions of 10 nm and beyond. For reflective optical systems, the challenge has been to achieve the desired optical shape ('figure') for imaging with a suitable bending, cutting, polishing or coating technique, while maintaining subnanometre surface roughness ('finish') over a broad spectral range. Errors in figure affect the image resolution in a manner similar to that of common aberrations, whereas surface roughness affects the contrast and throughput. Yamauchi, Mimura and colleagues, using crossed elliptical mirrors and a monochromator on an undulator beamline, demonstrated a spatial resolution of 30 nm with a 2D test pattern at 15 keV (ref. 32). More recently they have achieved 7 nm 1D focusing at 20 keV using an upstream deformable mirror and a multilayer coated KB mirror pair[21]. The multilayer coating allows for reflection at larger angles and thus provides a higher numerical aperture. With feedback from the focal region, the deformable mirror provides *in situ* wavefront correction, thus improving focusing.

X-ray microscopy methods

This section describes the basic principles of various X-ray microscopy methods, including transmission full-field X-ray microscopy (TXM), scanning transmission X-ray microscopy (STXM), scanning photoelectron microscopy, micro-X-ray fluorescence (μ-XRF) spectroscopy, and synchrotron radiation X-ray tomographic microscopy (SRXTM). The majority of these microscopes currently reside at synchrotron facilities, although promising advances in compact systems have been made and will be discussed later.

The full-field X-ray microscope, illustrated in Fig. 1e, is analogous to a visible-wavelength bright-field microscope. The sample is illuminated with quasi-monochromatic X-rays using a diffractive or capillary[33] condenser optic, and the X-rays transmitted from the sample are focused by an objective zone plate lens onto a CCD. The zone plate's outer zone width, illumination coherence and imaging geometry all contribute to the spatial resolution limit of the microscope. A hollow angular illumination cone — smaller than the numerical aperture of the zone plate and thus providing optimized partial coherence[34,35] — is often used, resulting in a spatial resolution somewhat better than Δr. For example, a zone plate that is broadly tunable but operating at a wavelength of 1.5 nm, with 500 zones and an outer zone width of 25 nm, would have a numerical aperture of 0.03, a diameter of 50 μm and a focal length of 0.83 mm. For example, a 2,000 × 2,000 pixel array with 1,000 photons per pixel, a zone plate efficiency of 10% and transmission of 50% requires about 10^{11} photons per image, although this rises to around 10^{12} when illumination optics are considered. An exposure time of several seconds is generally required for bending magnet synchrotron radiation. Resolution improvements through modified imaging configurations, such as the use of higher diffraction orders[36] or a compound zone plate[37], have been demonstrated. Phase-sensitive techniques such as Zernike phase contrast[38–42], differential interference contrast[43–46] and spiral phase contrast[47] have also been shown to provide improvements. 3D imaging is performed by first acquiring a series of 2D projection images at different sample angles and then applying tomographic reconstruction techniques.

In STXM (Fig. 1f), the radiation is focused by the zone plate to a small spot on the sample, following which the transmitted X-rays are detected. The sample is then two-dimensionally raster-scanned to form an image. The smallest spot size is achieved when the illuminating X-rays are spatially coherent[48], and when the scanning stage has suitable placement accuracy[49]. The point-to-point imaging process itself, however, is spatially incoherent. The typical spatial resolution is somewhat smaller than Δr. Using a zone plate with higher-order focusing can also help to improve the resolution, albeit with a reduction in efficiency. In the most common implementation of STXM, scanning the incoming photon energy by combining upstream undulator tuning and monochromatization provides spectral information for elemental and chemical speciation. Typical data accumulation times for undulator-based STXMs are of the order of one minute, depending on the sample size and the degree of spectral and spatial detail required. In this mode of operation the technique is often referred to as spectromicroscopy. Compared with TXM, STXM imaging requires a lower dose of radiation because the inefficiency of the lens is only incurred upstream of the sample and therefore does not affect the radiation dose.

Scanning photoemission microscopy[50], an alternative to the transmission-based imaging techniques described above, is a technique used to study a sample's surface state, surface composition and bonding. The optical configuration is similar to that of a scanning transmission X-ray microscope, but instead utilizing a photon-in electron-out mechanism rather than the measurement of transmitted radiation. The focusing optic is either a multilayer coated Schwarschild reflective optic, which provides high efficiency and long working distance but fixed-wavelength operation at lower photon energies, or a Fresnel zone plate, which provides a shorter working distance but broad spectral tunability. The electrons emitted from the sample surface are then collected and passed through an electron energy analyser.

Micro-X-ray fluorescence spectroscopy (Fig. 1g), a powerful tool for detecting trace elements, is performed by spectrally analysing emitted secondary photons as the sample is raster-scanned in front of a small X-ray focal spot. The incident photons knock out the core electrons from the various atoms present in the irradiated spot. The atoms then relax as an electron from an upper energy state drops into the vacancy, thereby emitting a fluorescent photon of characteristic energy for that particular element. Clearly the incident photon energy must be above that of the elemental binding energy of interest. By analysing the characteristic photon energies one can form an elemental map across the sample. This generally involves using bending magnet radiation and a KB mirror pair for focusing with multilayer coatings for photon energy selection. Because this is a photon-in photon-out technique, there is no bremsstrahlung radiation and thus very little background noise, permitting part-per-billion and femtogram sensitivities[51]. By adding an undulator and high-resolution monochromator, and instead detecting the transmitted rather than emitted photons (Fig. 1g), one attains the important capability of spatially resolved X-ray absorption spectroscopy. Micrometre-scale X-ray absorption near-edge spectroscopy (μ-XANES) is a particular variant of this technique that plays an important role in molecular, environmental and cultural heritage studies. Another variant, micrometre-scale X-ray diffraction (μ-XRD), permits localized structural determination.

Lastly, synchrotron radiation X-ray tomographic microscopy is a projection imaging technique in which the X-rays transmitted through a sample are imaged directly onto an array detector. 3D images are then reconstructed from the 2D projection datasets. This is often performed at micrometre-scale spatial resolutions using hard X-rays[52], with an increasing amount of research being performed at the submicrometre[53,54] level.

Materials science applications

Materials science is a great beneficiary of X-ray microscopy. The elemental specificity of soft X-rays and the tunability of synchrotron radiation together allow a variety of materials to be probed using spectromicroscopy. Scientifically and technologically interesting applications such as magnetic materials, solar cell defects and battery chemistry have so far been studied. Nanoscale magnetic materials are of interest for their basic physics and industrial importance as storage devices. Individual magnetic domains can be imaged using techniques such as TXM/STXM and photoemission electron microscopy. The primary contrast mechanism for ferromagnetic materials is X-ray magnetic circular dichroism[55–57], for example when the angular momentum of the absorbed photon is transferred to a $2p$ electron, permitting its transition to a $3d$ state in transition metals. Local differences in the dot product of the magnetization direction and the direction of the incoming light provide image contrast between different magnetic domains. Sources such as off-axis bending magnets and elliptical undulators can provide the necessary degree of circular polarization[58,59]. X-ray polarization filters[60] have also been developed for the conversion of linearly to circularly polarized radiation. Of particular interest is the ability to image magnetic domains of various materials at high spatial and temporal resolutions. Dynamical studies of switching are performed today using TXM and STXM pump–probe set-ups with time resolutions of around 100 ps (limited by the pulse structure of the synchrotron). Figure 2a shows an X-ray magnetic circular dichroism image from a study of vortex dynamics[61] in a confined rectangular geometry of permalloy ($Ni_{80}Fe_{20}$). In a video of such images, with frames 500 ps apart, one can see the crossed pattern of Fig. 2a dancing laterally, from left to right, driven by the magnetic fields associated with repetitive current pulses. Magnetic

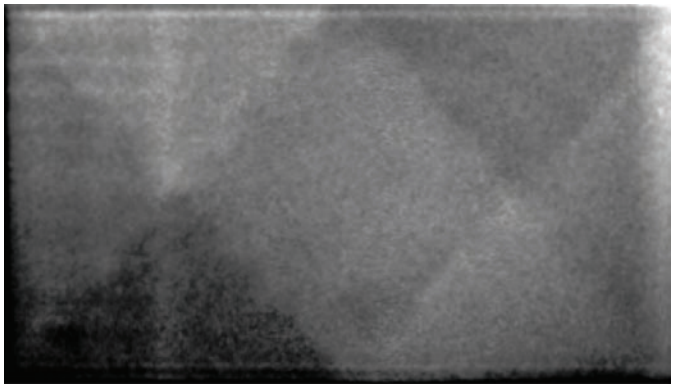

Figure 2 | Materials science applications of nanoscale X-ray imaging. Time-resolved soft-X-ray studies of vortex dynamics at the Fe K-absorption edge (707 eV) in a rectangular permalloy sample ($Ni_{80}Fe_{20}$) measuring 2 μm × 4 μm × 100 nm. Vortex dynamics are visualized in an online video clip, which shows the vortices dancing laterally in response to repetitive 100 ps rise-time current excitation pulses. The external field used to saturate the sample is along the long axis, whereas the exciting magnetic field, driven by current pulses, is along the short axis. The video frames were taken at 500 ps intervals at the Advanced Light Source full-field soft-X-ray microscope XM1. Each frame consists of photons from a series of 70 ps soft-X-ray pulses. Figure reproduced with permission from ref. 61, © 2007 AVS.

transmission soft-X-ray microscopy studies such as this are limited in terms of the sample preparation, as only substrates thin enough to transmit soft-X-rays near the appropriate absorption edges are compatible. Novel magnetic materials are generally not compatible with transmission soft-X-ray microscopy as they are grown epitaxially on thick substrates that are opaque to soft X-rays, thus currently limiting the range of magnetic materials available for such studies, but work in sample preparation and reflection imaging techniques are being pursued.

An interesting industrial application of μ-XRF spectroscopy is the detection of metallic impurities in solar cells, devices that convert solar energy into electricity through the photoelectric effect. Although solar cells are typically made from highly purified polycrystalline silicon — an expensive material — lower-cost alternatives such as 'solar-grade silicon' contain trace amounts of transition metal impurities. A minute concentration (<1 part per 10^9) of iron-containing metal clusters, for example, can drastically reduce the efficiency of a solar cell[62]. Buonassisi *et al.* have used μ-XRF spectroscopy to determine the size and spatial distributions of metal defects within commercial and next-generation solar-cell materials, with the goal of producing devices that convert sunlight to electricity in an economically competitive manner[63,64].

The role of batteries for applications such as transportation, electronics and cell phones increases in importance year after year. Fuel cells and batteries involve nanoscale electrochemical surface phenomena, which can be characterized using X-ray microscopy. Effective catalysis in a fuel cell requires the transport of electrons and ions, thus placing particular importance on studies of the porosity, chemical states and the particle sizes of the elements involved. Such characterizations, as a function of reaction conditions, can be very valuable. Optimizing the charge–discharge cycle of a battery requires the electrode oxidation states to be determined and correlated with the morphological changes. 2D and 3D chemical mappings, obtained by combining XANES and tomographic imaging at the Ni K-edge, have been used to determine oxidation state, particle size distribution and electrode porosity as a function of charge for Li–NiO battery electrodes. The 3D XANES[65] technique is proving to be very valuable as a tool for the design of highly efficient, cost-effective batteries.

Biological applications

Microscopy has been a fundamental tool for biologists for over a century. With visible light and fluorescence microscopy, biologists have been able to visualize cell dynamics and the functionality of various proteins with conventional resolutions of around 200 nm. Recent advances in super-resolution fluorescence techniques such as structured illumination[66], stimulated emission depletion[67] and stochastic optical reconstruction microscopy/photoactivated localization microscopy have enabled objects to be imaged down to a few tens of nanometres. Electron microscopy, on the other hand, is used to image ultrastructure at nanometre resolution, albeit with long imaging times and intensive sample preparation, including chemical fixation, staining and sectioning — all of which can lead to artefacts. Complimenting the valuable and well-developed roles of fluorescence and electron microscopes, X-ray microscopy offers advantages in visualizing unsectioned, frozen-hydrated whole cells using natural contrast and short imaging times with 3D resolutions of the order of tens of nanometres.

Soft-X-ray TXM/STXM within the water window can be used to study frozen-hydrated cells typically ~10 μm thick using natural absorption contrast. Although the effects of radiation dose and damage can be mitigated[68] through cryofixation, care must be taken to avoid nanocrystalline ice formation, which leads to imaging artefacts. 3D imaging[69] is achieved through sequential 2D imaging of rotated samples, followed by computed tomography image-reconstruction techniques, and can be performed in several minutes. This technique, when combined with minimal sample preparation, makes it an attractive candidate for detailed, high-throughput studies. Contrast, dose and depth-of-field limit the effective resolution available, particularly for the tomographic imaging of thicker samples. Molecular localization is possible through immunogold or other labelling protocols, and future developments in multimodality microscopy, for example between X-ray and fluorescence microscopy[70], may provide significant insights through the correlation of different types of information, such as structure and function.

Among the many areas currently being pursued is the study of the structural pathology of subcellular features in diseased cells. Schneider *et al.* performed tomography on a mouse adenocarcinoma cell[71] using TXM at 510 eV with an objective lens of $\Delta r = 25$, together with a flat sample holder with a tilt capability of ±60° in 1° increments. Because the cell was grown on a flat substrate, a full tomographic dataset was not obtained, resulting in the 'missing wedge' problem, which is common in electron tomography. Nevertheless, high-resolution 2D slices from a reconstructed tomogram revealed subcellular structure, including mitochondria, lysosomes, endoplasmic reticulum, vesicles, nuclear pores and a 29 nm double-layer nuclear membrane.

The high-throughput capability of soft-X-ray tomography allows for statistical studies of structural differences between normal and mutated genes. Yeast cells are widely used as models for genetic studies. Utilizing a hollow capillary sample holder to achieve full tomographic data sets with a full-field X-ray microscope, Larabell *et al.* obtained images of whole, fully hydrated, unstained and cryofixed yeast *Schizosaccharomyces pombe*[72,73]. Images were taken at 517 eV with Δr = 45 nm, over a ±90° angle in 2° increments. Figure 3a,b shows a 2D slice of a not-yet-separated mother–daughter yeast cell pair and the corresponding 3D reconstructed tomogram. Cellular substructure is colour-coded according to the attenuation coefficient, and those of a similar colour are identified as particular organelle types. Earlier work by Meyer-Ilse *et al.* demonstrated the possibilities for molecular localization through the immunogold labelling of

NATURE PHOTONICS DOI: 10.1038/NPHOTON.2010.267

specific proteins[74]. In Fig. 3c, silver-enhanced gold labelling was used to visualize the microtubule network in a whole, hydrated mouse epithelial cell[74].

Compared with soft X-rays, Hard X-rays are advantageous for biological X-ray tomography because they allow deeper penetration into larger-scale structures such as tissue and organs, as well as having more favourable conditions (less absorption) for use in phase-sensitive techniques. Stampanoni *et al.* demonstrated X-ray tomography at 25 keV in a wide range of bone and vascular structures[75]. Figure 3d shows the microvascular structure of a mouse brain, obtained using synchrotron radiation X-ray tomographic microscopy. The rendering of the microvascular architecture shows small capillaries in blue and larger blood vessels in red.

Environmental science applications

Environmental science is an interdisciplinary field addressing problems — both fundamental and applied — that impact human health and welfare. Communities across the globe face the daunting task of characterizing, treating and/or disposing of vast quantities of contaminated materials, including mining and industrial wastes, atmospheric pollutants and agricultural chemicals[76]. A particular problem is that of concrete formation[77], a resource-intensive process that produces a large share of the world's CO_2 emissions. The 11.5 billion tons of concrete produced each year consume tremendous resources: 1.5 billion tons of cement, 1 billion tons of water and 9 billion tons of sand and rock. Potential solutions are being explored in many areas, ranging from the use of geopolymers to the recycling of fly ash. Monteiro *et al.* have used X-ray microscopy to perform *in situ* investigations of nanostructure formation and evolution within cement, yielding surprising and very valuable insights to the hydration process, including direct nanoscale views of the onset of crack formation[78]. In more recent work[79], illustrated in Fig. 4a–d, expansive cements containing the admixture C_4A_3S, which is used to alleviate cracking, were studied to determine morphology as a function of chemistry.

Aluminium toxicity in plants is a worldwide agricultural problem that limits the performance of crops in acidic soil. Toxicity occurs when the soil pH drops below 5 and the aluminium becomes soluble in the form of Al^{3+}, resulting in the inhibition of root growth and ultimately in the degradation of plant health. Interestingly, certain vegetation such as the tea plant are tolerant to these conditions, and considerable research over the past few decades has led to a better understanding of the mechanisms behind this. Being able to visualize the distribution of various elements within plant cells can contribute to a fuller understanding of these mechanisms and potentially help to develop future solutions to alleviating aluminium toxicity in plants. Using low-energy X-ray fluorescence spectroscopy[80], cryofixed freeze-dried tea (*Camellia sinensis*) leaf cross-sections of the mesophyll and xylem phloem regions, approximately 2 mm × 2 mm and 20 μm thick, have been imaged[81]. Energies used were in the range of 1.7–2.2 keV — covering the absorption edges of Al, C, O, Mg, Si and P — and imaging was performed with 10 ppm sensitivity at a spatial resolution of 1 μm. An elemental map of aluminium retention within these regions of the leaves is shown in Fig. 4e–h.

There are many further applications of X-ray imaging to plant biology and environmental sciences. For example, Hitchcock and colleagues have studied river pollution and bioremediation processes using scanning transmission X-ray spectromicroscopy[82,83]. In a particular study of biofilms from the Saskatoon river, the researchers generated elemental maps of Ni, Fe, Mn, Ca, K, O and C, as well as their various oxidation states, to better understand the role of microbial biofilms in processes affecting metal toxicity and bioavailability in the hydrosphere. Significant differences between the distributions of Fe and those of Ni and Mn suggested that different bacterial species, each with unique polysaccharides, exhibit significant variation in their affinity for specific metals, offering a potential path for bioremediation[84]. Another study utilized a tomographic extension of spectromicroscopy to investigate the early stages of biomineralization in freshwater cyanobacteria, *Synechococcus leopoliensis* PCC 7942, to better understand the mechanisms of biomediated calcium carbonate nucleation and growth. Facilitating such biocalcification mechanisms has been proposed as a method for carbon sequestration, but the exact mechanisms are not yet fully understood. From this study, amorphous aragonite-like calcium carbonate was homogenously precipitated in the extracellular polysaccharide layer closest to the cell. Calcite, a polymorph of calcium carbonate that is more thermodynamically stable and less soluble than calcium carbonate itself, was occasionally formed.

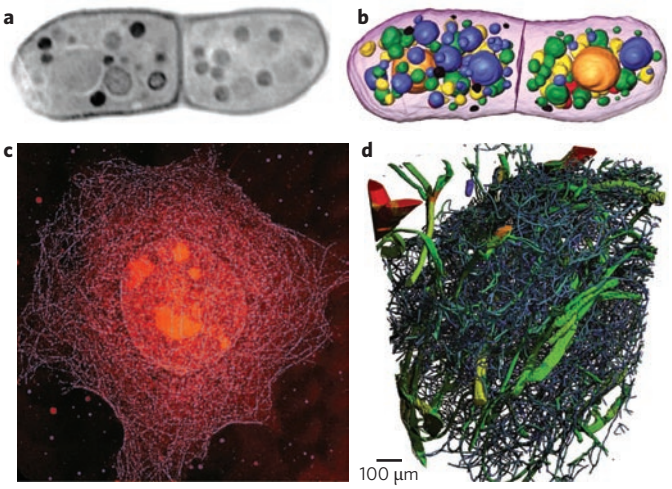

Figure 3 | Biological applications of nanoscale X-ray imaging. a,**b**, A not-yet-separated mother–daughter yeast cell pair, whole and unstained with rapid-freeze cryofixation. Yeast cells are important because they are used as biological model systems for genetic studies. These projection 2D images were taken with a zone plate of 45 nm outer zone width, at 2° intervals covering an angle of 180°, at 517 eV (wavelength of 2.4 nm). Figure **a** shows a soft-X-ray image of an 8.5-μm-wide yeast cell, *Schizosaccharomyces pombe*, extracted as a 2D slice of a reconstructed 3D tomogram obtained at the National Center for X-Ray Tomography full-field microscope at the Advanced Light Source. The image shows a one-voxel-thick slice with grey-scale values corresponding to the observed X-ray absorption coefficient. Figure **b** shows the same cell pair, with sub-cellular components of similar colour correlated according to X-ray attenuation. **c**, The important technique of protein-specific labelling. X-ray absorptive nanoparticles are used to visualize a microtubule network in a whole, hydrated, but chemically fixed EPH4 mouse epithelial cell. The label consists of a silver-enhanced gold nanoparticle of 50 nm diameter, which roughly matches the spatial resolution of the microscope. The image measures 10 μm^2, and was taken at a resolution of 36 nm and a photon energy of 517 eV. Absorption-dependent quantitative colour-coding is used for visualization. The highly absorbing gold/silver labels in blue highlight the linear microtubule network against a less absorptive (and unlabeled) nuclear structure, shown in orange. The relatively high-water-content cytoplasm has low absorption and so appears black. **d**, Hard-X-ray 3D tomographic rendering of the microvascular architecture within the hippocampus region of a mouse brain. Small capillaries are shown in blue, whereas larger blood vessels are shown in red. The reconstructed volume is a cube of 700 μm × 700 μm × 700 μm. A photon energy of 25 keV was use to obtain the data. The spatial resolution is approximately 15 μm. Figure reproduced with permission from: **a**,**b**, ref. 97, © 2008 Elsevier; **c**, ref. 74, © 2001 Wiley. Figure **d** courtesy of M. Stampanoni

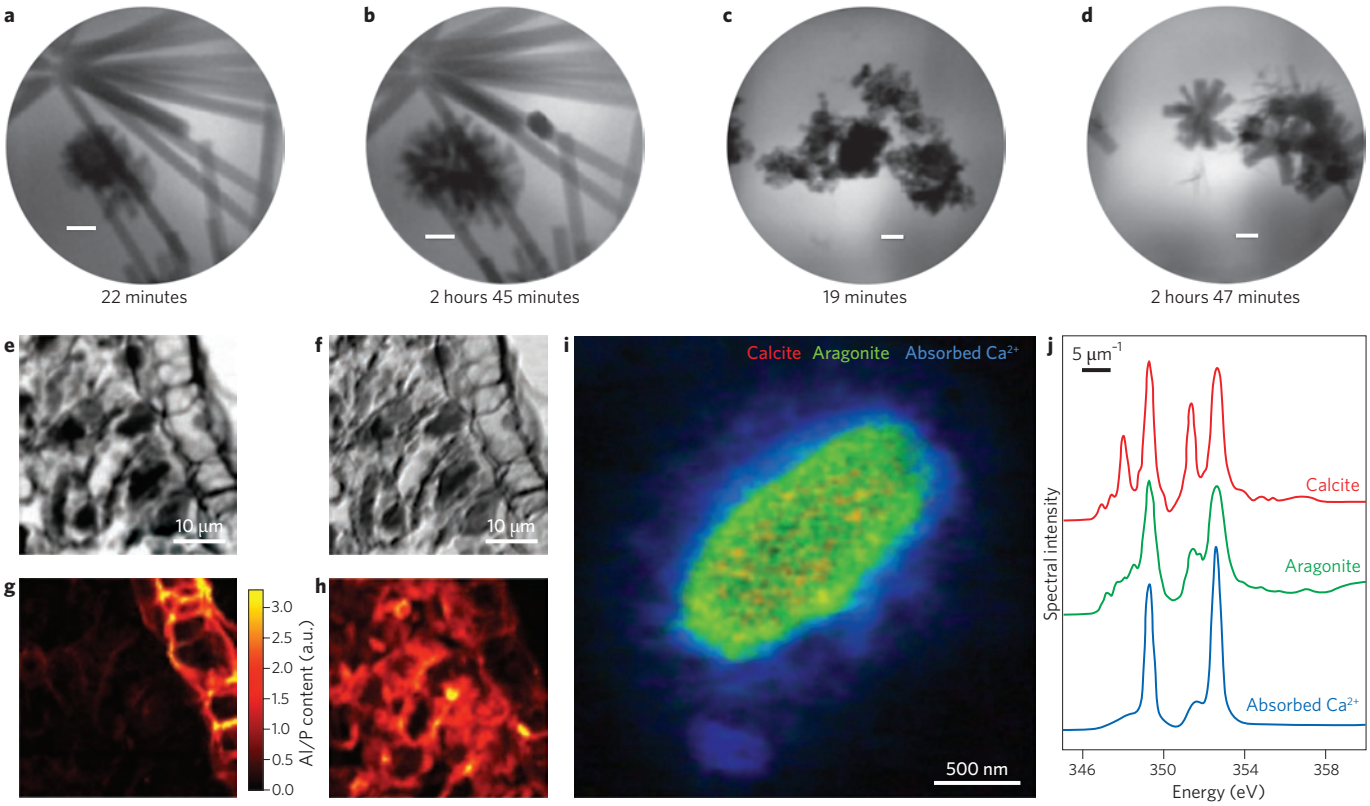

Figure 4 | Environmental applications of nanoscale X-ray imaging. Concrete formation is a major source of air and water pollution. **a**–**d**, Studies of expansive cements containing the admixture C_4A_3S, which is used to alleviate cracking, to determine the morphology as a function of chemistry. In the formula C_4A_3S, C refers to calcium (Ca), A to alumina (Al_2O_3) and S to silica (SiO_2). These soft-X-ray images show the emergence of large ribbon-like structures of hydrating C_4A_3S particles, in fan-like configurations, in saturated solutions of $Ca(OH)_2$ + $CaSO_4{\cdot}H_2O$, as a function of hydration time. Images are in the absence (**a**,**b**) and presence (**c**,**d**) of 10% $Ca(OH)_2$. The images show how ribbon size is strongly affected by chemistry. The images were obtained at 520 eV (wavelength of 2.4 nm) using the full-field soft-X-ray microscope at the Advanced Light Source. The scale bars are 1 μm wide. **e**–**h**, The study of aluminium toxicity in tea leaves (*Camellia sinensis*) using X-ray images and elemental maps at 1.7–2.2 keV. Slices of tea leaves reveal that the aluminium concentration is high in the epidermal (Epi) cell walls but low in the mesophyll (Mes) cell walls. The much lower content of phosphorous in the epidermal cells compared with the mesophyll cells indicates that phosphorous plays a negligible role in the sequestration of aluminium. Figure **e**,**f** shows brightfield (BF) and differential phase contrast (DPC) X-ray images of slices from tea leaves, respectively. Figure **g**,**h** shows aluminium and phosphorus low-energy X-ray fluorescence maps, respectively. **i**,**j**, From studies of pollution and potential carbon sequestration in the hydrosphere, STXM soft-X-ray spectromicroscopy is used to map concentrations of calcite, aragonite and calcium ions in the extracellular polysaccharide matrix of freshwater cyanobacteria *Synechococcus leopoliensis*. Calcite is shown in red, aragonite in green, and adsorbed calcium ions in blue. Curves are arbitrarily separated vertically for visual clarity. Figure reproduced with permission from: **a**–**d**, ref. 79, © 2009 Elsevier; **e**–**h**, ref. 81, © 2010 Springer; **i**,**j**, ref. 82, © 2009 Elsevier.

Figure 4i,j shows absorption spectra and chemical maps of Ca ions, calcite and aragonite (polymorphs of calcium carbonate) in the extracellular polysaccharide matrix of the cyanobacteria[82,83].

Archaeology, palaeontology and heritage applications

Several interesting applications of X-ray spectromicroscopy techniques involve the dating, provenance, authentication and restoration of items collectively described as cultural heritage. Here, the non-invasive nature and high spatial resolution of X-ray spectromicroscopy, combined with techniques such as X-ray fluorescence (for elemental identifications, often to trace amounts), diffraction (for structural phase information) and absorption spectroscopy (information on the chemical state and environment) provide significant tools for studies in the field of cultural heritage[85–87]. In early work, Underwood and Thompson used a multilayer coated KB μ-XRF microscope to study ink characteristics for authenticating medieval documents, detecting arsenic concentrations in Napoleon's hair and providing an elemental analysis of the poison in a spider's fang[62]. As an example, Fig. 5a,b shows an Egyptian opaque coloured glass vase from around 1400 BC, for which μ-XANES, μ-XRF spectroscopy and μ-XRD have been used to study the role of calcium antimonates in opacified glasses by measuring antimony concentrations and chemical states, along with the role and structure of crystalline additives in the fabrication, transparency and colour of such ancient vases[88]. Donoghue and colleagues used SRTXM to study the anatomical structure of fossilized animal embryos[89] from the Precambrian period (about 500 million years ago), during which diverse forms of life first appeared. These fragile embryos are among the oldest known, and are only a few hundred micrometres in diameter. Figure 5c shows a tomographic reconstruction of a fossilized embryo of *Markuelia hunanensis*, a 520-million-year-old relative of modern roundworms and arthropods. Visualization of the interior structure provides significant insight into the developmental processes in these early stages of animal diversification, and could not have been obtained through any other method. Bergmann and colleagues used μ-XRF spectroscopy to study the evolutionary link between birds and dinosaurs through the detailed chemical analysis of 150-million-year-old fossil remains of *Archaeopteryx* feathers and bones[90]. More recently, Bergmann and colleagues used μ-XRF spectroscopy to investigate the Archimedes' treatise[90,91], which can be traced back to around

NATURE PHOTONICS DOI: 10.1038/NPHOTON.2010.267

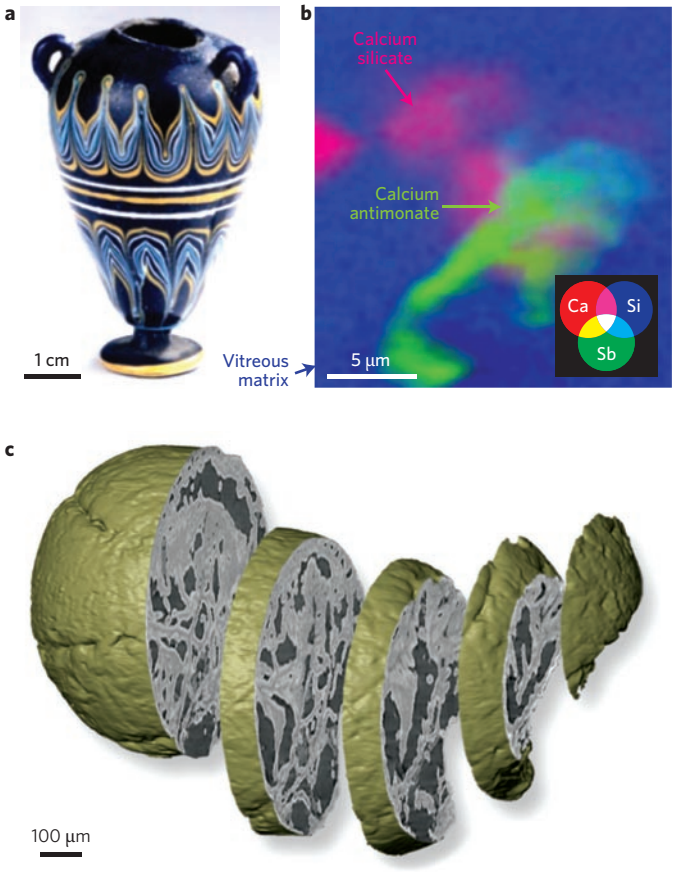

Figure 5 | Archaeological and paleontological applications of microscale X-ray imaging. a, An 18th dynasty Egyptian glass vase studied for its colour and opaqueness, attributes that are determined by the chemical properties of the contained nanoparticles. Research at the European Synchrotron Radiation Facility included the use of μ-XRF spectroscopy, μ-XANES and μ-XRD to study the elemental composition and oxidation states of antimony in the vitreous matrix. **b**, Colour-coded X-ray fluorescence mapping showing the elemental distribution of calcium (Ca), antimony (Sb), and silicon (Si). Detailed μ-XANES measurements (not shown) were made in the vicinity of the Sb $L_{1\text{-edge}}$ at 4.7 keV. The microprobe beam size was 1.1 μm × 0.3 μm. Micrometric devitrification crystals (calcium silicates) as well as opacification crystals (calcium antimonate) were identified. **c**, Tomographic reconstruction of a fossilized embryo of *Markelia hunanensis,* a 520-million-year-old relative of modern roundworms and arthropods that was found in southern China. The fragile embryos are only a few hundred micrometres across. This synchrotron radiation X-ray tomographic microscopy data was obtained at the Swiss Light Source's Tomcat beamline, at an energy of 17.5 keV. Reconstructed images reveal details of the mouth, teeth and gut that could not have been resolved by any other non-destructive technique. Interpretation of the data permitted the authors to test theories relating to the biological affinities of these early embryos with those of other life forms in the evolutionary path. Figure reproduced with permission from: **a**,**b**, ref. 88, © 2010 Springer; **c**, ref. 89, © 2006 NPG.

third century BC. Many other contributions to cultural heritage now regularly appear in the literature, with relevant capabilities at all the major synchrotron radiation facilities.

Compact X-ray microscopy

Much of our science and technology is developed in small laboratories; in university, clinical and industrial settings. This Review has shown that the scientific and technological applications of X-ray

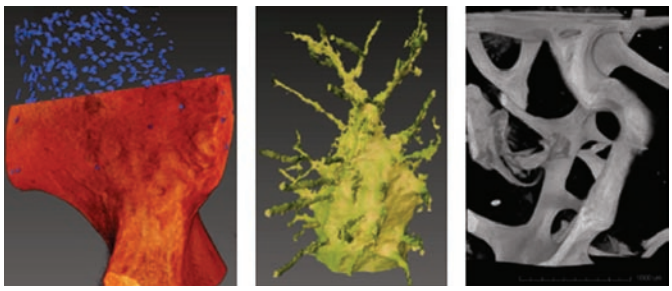

Figure 6 | 3D rendered images of a mouse bone. Image resolutions are 3 μm (left), 1 μm (middle) and 150 nm (right). The tomograms were obtained using a compact, laboratory-scale X-ray microscope operating at 8 keV. Figure courtesy of M. Schaffler and W. Yun.

microscopy are extremely diverse, and similar capabilities with compact X-ray microscopes would support a far broader use of X-ray microscopy. Efforts are being made towards the development of such compact systems, both in universities and small businesses. The main issue is the development of compact high-brightness X-ray sources that permit exposure times of seconds to minutes. The technical capabilities of synchrotron-based microscopes, such as the use of zone plates, can be directly translated for use with compact sources. The combination of microscopy and spectroscopy requires a substantial photon flux, which so far has only been available at larger facilities. Compact microscopes currently have longer exposure times than their synchrotron counterparts, but significant progress has been made over the past decade towards improving the available fluxes. This burden can also be alleviated through use of higher-efficiency optics.

Hertz and colleagues have been developing microscopes[92,93] based on compact laser-produced plasma sources through a variety of creative approaches. Soft X-rays have been generated using a liquid-jet laser–plasma source[94], in which a jet of small liquid droplets is laser irradiated at a wavelength that is dependent on the composition of the droplets. In the hard-X-ray region — around 9–25 keV — electron-impact liquid-metal-jet-anode X-ray sources[95] have been shown to provide a brightness >10 times higher than current microfocus tubes. Such sources have been engineered into imaging systems to create compact high-resolution X-ray microscopes.

The company Xradia has been leading the effort in the development and commercialization of hard-X-ray synchrotron-based and compact X-ray microscopes. Their compact microscopes are based on currently available microfocus sources, and have been used in a wide range of applications ranging from biological, environmental and materials science to semiconductor inspection. Both micrometre-scale imaging systems similar to SRXTM, except using a compact source, and nanoscale imaging systems, using zone plate lenses, have been developed. Figure 6 shows tomographic images of a mouse bone taken using Xradia's compact X-ray microscope.

Perspectives

Improvements in X-ray imaging techniques are ongoing and will undoubtedly provide major enhancements to the breadth of scientific and technological applications at existing synchrotron facilities. Such techniques will also have a significant impact on femtosecond-duration X-ray sources, permitting time-resolved dynamical studies, and compact high-brightness X-ray sources, which would make X-ray microscopy available to a much broader community.

At existing synchrotrons, we can expect significant scientific advances based on improvements in X-ray imaging techniques, particularly as X-ray imaging is accepted into the larger community and combined with other modalities. This would potentially include

higher-resolution X-ray imaging in two and three dimensions, further development of contrast-enhancing techniques, effective combinations of imaging modalities, and advanced imaging schemes. New or improved nanofabrication processes and capabilities will benefit all of the above. As the community pursues higher-resolution imaging, more critical evaluation must be given to the trade-offs and requirements of resolution, contrast and dose. Imaging at higher resolution will require improved sample contrast, which in turn could require a large number of photons per voxel to keep statistical noise levels low, and this could result in a much higher dose. For this reason, contrast-enhancing methods such as labelling may play a more prominent role in visualizing small structures in radiation-sensitive samples.

Recent progress in the development of X-ray free-electron lasers[96] has demonstrated the capability for producing intense, high-brightness X-ray pulses of femtosecond duration, with the potential for achieving attosecond durations in the future. Scientific experiments that would benefit from this new capability include switching processes in magnetic materials, which are believed to be on timescales of 10–20 fs, electron dynamics in chemical systems, which occur on femto- and attosecond timescales, and studies of correlated solid-state phenomena, which require angular-resolved photoemission with both spatial and temporal resolution. Such studies will require further developments in the reflective and diffractive optics. For example, temporal pulse shaping optics, diffractive focusing optics, thin-film beamsplitters and dichroic optical elements for pump–probe experiments will be needed. Although the optics in a free-electron laser beam often suffer from radiation damage, there are situations in which an optic can be designed to survive. Clearly there are many opportunities in this field that will require both nanometre spatial resolution and femtosecond time resolution.

In this Review we have selected a few examples that illustrate the substantial scientific progress being made in the utilization of X-ray imaging, both at the nano- and microscale. The number of applications is growing rapidly as synchrotron radiation facilities appear around the world, some of which have a variety of X-ray imaging techniques. Furthermore, the range of scientific questions that can be addressed is increasing as our imaging capabilities improve. Continued progress in the development of compact X-ray microscopy will support the participation of a wider range of university, clinical and industrial researchers, and the emergence of intense, femtosecond-duration sources will open completely new opportunities for dynamical studies in the realm of nanometre and femtosecond science.

References

1. Attwood, D. T. *Soft X-rays and extreme ultraviolet radiation: Principles and applications* Ch. 1–9 (Cambridge Univ., 1999).
2. Kirkpatrick, P. & Baez, A. V. Formation of optical images by X-rays. *J. Opt. Soc. Am.* **38,** 766–773 (1948).
3. Baez, A. V. Fresnel zone plate for optical image formation using extreme ultraviolet and soft X radiation. *J. Opt. Soc. Am.* **51,** 405–412 (1961).
4. Schmahl, G. (ed.) X-ray microscopy. *Proc. Int. Symp.* (Springer, 1983).
5. Sayre, D., Howells, M., Kirz, J. & Rarback, H. (eds) X-ray Microscopy II. *Proc. Int. Symp.* (Upton, 1987).
6. Kirz, J., Jacobsen, C. & Howells, M. Soft X-ray microscopes and their biological applications. *Q. Rev. Biophys.* **28,** 33–130 (1995).
7. Aoki, S. (ed.) *Proc. 8th Int. Conf. X-ray Microscopy* (IPAP, 2005).
8. Eichert, D. *et al.* Imaging with spectroscopic micro-analysis using synchrotron radiation. *Anal. Bioanal. Chem.* **389,** 1121–1132 (2007).
9. David, C. (ed.) *Proc. 9th Int. Conf. X-ray Microscopy* (IOP, 2008).
10. Schmahl, G. & Rudolph, D. Lichtstarke zonenplatten als abbildende systeme für weiche Röntgenstrahlung. *Optik* **29,** 577–585 (1969).
11. Niemann, B., Rudolph, D. & Schmahl, G. X-ray microscopy with synchrotron radiation. *Appl. Opt.* **15,** 1883–1884 (1976).
12. Rarback, H. *et al.* Scanning X-ray microscope with 75-nm resolution. *Rev. Sci. Instrum.* **59,** 52–59 (1988).
13. Kirz, J. *et al.* X-ray microscopy with the NSLS soft X-ray undulator. *Phys. Scripta* **T31,** 12–17 (1990).
14. Ojeda-Castañeda, J. & Gomez-Reino, C. (eds.) *Selected papers on zone plates* (SPIE, 1996).
15. Vila-Comamala, J. *et al.* Advanced thin film technology for ultrahigh resolution X-ray microscopy. *Ultramicroscopy* **109,** 1360–1364 (2009).
16. Chao, W., Kim, J., Rekawa, S., Fischer, P. & Anderson, E. H. Demonstration of 12 nm resolution Fresnel zone plate lens based soft X-ray microscopy. *Opt. Express* **17,** 17669–17677 (2009).
17. Schwarzschild, K. Untersuchungen zur geometrischen optic II. Astronomische Mitteilungen der Kniglichen Sternwarte zu Göttingen. **10,** 4–28 (1905).
18. Cerrina, F. *et al.* Maximum: A scanning photoelectron microscope at Aladdin. *Nucl. Instrum. Meth. A* **266,** 303–307 (1988).
19. Wolter, H. Spiegelsystems streifenden einfalls als abbildende optiken für Röntgenstralen. *Ann. Physik* **10,** 94–114 (1952).
20. Aoki, S. in *X-ray Microscopy II* (ed. Sayre, D.) 102 (Springer, 1988).
21. Mimura, H. *et al.* Breaking the 10 nm barrier in hard-X-ray focusing. *Nature Phys.* **6,** 122–125 (2010).
22. Snigirev, A., Kohn, V., Snigireva, I. & Lengeler, B. A compound refractive lens for focusing high energy X-rays. *Nature* **384,** 49–51 (1996).
23. Snigirev, A., Kohn, V., Snigireva, I., Souvorov, A. & Lengeler, B. Focusing high-energy X-rays by compound refractive lenses. *Appl. Opt.* **37,** 653–662 (1998).
24. Bosak, A., Snigireva, I., Napolskii, K. S. & Snigirev, A. High-resolution transmission X-ray microscopy: A new tool for mesoscopic naterials. *Adv. Mater.* **22,** 3256–3259 (2010).
25. Yin, G.-C. *et al.* Sub-30 nm resolution X-ray imaging at 8 keV using third order diffraction of a zone plate lens objective in a transmission microscope. *Appl. Phys. Lett.* **89,** 221122 (2006).
26. Chapman, H. N. & Nugent, K. A. Coherent lensless X-ray imaging. *Nature Photon.* **4,** 833–839 (2010).
27. Vila-Comamala, J. *et al.* Dense high aspect ratio hydrogen silsesquioxane nanostructures by 100 keV electron beam lithography. *Nanotechnology* **21,** 285305 (2010).
28. Maser, J. *et al.* Near-field stacking of zone plates for hard X-ray range. *Proc. SPIE* **4783,** 74–81 (2002).
29. Chao, W., Harteneck, B. D., Liddle, J. A., Anderson, E. H. & Attwood, D. T. Soft X-ray microscopy at a spatial resolution better than 15 nm. *Nature* **435,** 1210–1213 (2005).
30. Kang, H. C. *et al.* Focusing of hard X-rays to 16 nanometers with a multilayer Laue lens. *Appl. Phys. Lett.* **92,** 221114 (2008).
31. Yan, H. X-ray nanofocusing by kinoform lenses: A comparative study using different modeling approaches. *Phys. Rev. B.* **81,** 075402 (2010).
32. Matsuyama, S. *et al.* Development of scanning X-ray fluorescence microscope with spatial resolution of 30 nm using Kirkpatrick–Baez mirror optics. *Rev. Sci. Instrum.* **77,** 103102 (2006).
33. Zeng, X. *et al.* Ellipsoidal and parabolic glass capillaries as condensers for X-ray microscopes. *Appl. Opt.* **47,** 2376–2381 (2008).
34. Born, M. & Wolf, E. *Principles of Optics* (Cambridge Univ., 1999).
35. Jochum, L. & Meyer-Ilse, W. Partially coherent image formation with X-ray microscopes. *Appl. Opt.* **34,** 4944–4950 (1995).
36. Yin, G. C. *et al.* Energy-tunable transmission X-ray microscope for differential contrast imaging with near 60 nm resolution tomography. *Appl. Phys. Lett.* **88,** 241115 (2006).
37. von Hofsten, O. *et al.* Sub-25 nm laboratory X-ray microscopy using a compound Fresnel zone plate. *Opt. Lett.* **34,** 2631–2633 (2009).
38. Schmahl, G., Rudolph, D., Schneider, G., Guttmann, P. & Niemann, B. Phase contrast X-ray microscopy studies. *Optik* **97,** 181–182 (1994).
39. Schmahl, G. *et al.* Phase contrast studies of biological specimens with the X-ray microscope at BESSY. *Rev. Sci. Instrum.* **66,** 1282–1286 (1995).
40. Yokosuka, H. *et al.* Zernike-type phase-contrast hard X-ray microscope with a zone plate at the Photon Factory. *J. Synchrotron Rad.* **9,** 179–181 (2002).
41. Youn, H. S. & Jung, S.-W. Hard X-ray microscopy with Zernike phase contrast. *J. Microsc.* **223,** 53–56 (2006).
42. Sakdinawat, A. & Liu, Y. Phase contrast soft X-ray microscopy using Zernike zone plates. *Opt. Express* **16,** 1559–1564 (2008).
43. Wilhein, T., Kaulich, B., Di Fabrizio, E. & Romanato, F. Differential interference contrast X-ray microscopy with submicron resolution. *Appl. Phys. Lett.* **78,** 2082–2084 (2001).
44. Kaulich, B. *et al.* Differential interference contrast X-ray microscopy with twin zone plates. *J. Opt. Soc. Am. A* **19,** 797–806 (2002).
45. Di Fabrizio, E. *et al.* Diffractive optical elements for differential interference contrast X-ray microscopy. *Opt. Express* **11,** 2278–2288 (2003).
46. Chang, C., Sakdinawat, A., Fischer, P., Anderson, E. H. & Attwood, D. T. Single-element objective lens for soft X-ray differential interference contrast microscopy. *Opt. Lett.* **31,** 1564–1566 (2006).
47. Sakdinawat, A. & Liu, Y. Soft-X-ray microscopy using spiral zone plates. *Opt. Lett.* **32,** 2635–2637 (2007).

48. Attwood, D., Kim, K.-J. & Halback, K. Tunable Coherent Radiation. *Science* **228,** 1265–1272 (1985).
49. Tyliszczak, T., Kilcoyne, A., Warwick, A., Liddle, A. & Shuh, D. High spatial resolution scanning transmission X-ray microscope at the Advanced Light Source. *Proc. 8th Int. X-ray Microscopy Conf.* 88 (IPAP, 2006).
50. Barinov, A. *et al.* Synchrotron-based photoelectron microscopy. *Nucl. Instrum. Meth. A* **601,** 195–202 (2009).
51. Thompson, A. & Underwood, J. H. in *Soft X-rays and Extreme Ultraviolet Radiation* 117 (Cambridge Univ., 1999).
52. Stampononi, M. *et al.* Trends in synchrotron-based tomographic imaging: the SLS experience. *Proc. SPIE* **6318,** 63180M (2006).
53. Requena, G. *et al.* Sub-micrometer synchrotron tomography of multiphase metals using Kirkpatrick-Baez optics. *Scripta Mater.* **61,** 760–763 (2009).
54. Stampanoni, M. *et al.* Phase-contrast tomography at the nanoscale using hard X-rays. *Phys. Rev. B.* **81,** 140105 (2010).
55. Thole, B. T., Carra, P., Sette, F. & van der Laan, G. X-ray circular dichroism as a probe of orbital magnetization. *Phys. Rev. Lett.* **68,** 1943–1946 (1992).
56. Stöhr, J. & Siegmann, H. C. *Magnetism: from Fundamentals to Nanoscale Dynamics* (Springer, 2006).
57. Schutz, G., Goerning, E. & Stoll, H. in *Handbook of Magnetism and Advanced Magnetic Materials* (eds. Kronmueller, H. & Parkin, S.) 1309–1363 (Wiley, 2007).
58. Kim, K.-J. Polarization characteristics of synchrotron radiation sources and a new two undulator system. *Nucl. Instrum. Meth.* **222,** 11–13 (1984).
59. Hofmann, A. *The Physics of Synchrotron Radiation* (Cambridge Univ., 2007).
60. Pfau, B. *et al.* Magnetic imaging at linearly polarized X-ray sources. *Opt. Express* **18,** 13608–13615 (2010).
61. Mesler, B. L., Fischer, P., Chao, W., Anderson, E. H. & Kim, D.-H. Soft X-ray imaging of spin dynamics at high spatial and temporal resolution. *J. Vac. Sci. Technol. B* **25,** 2598–2602 (2007).
62. Underwood, J. H., Thompson, A., Wu, Y. & Giauque, R. D. X-ray microprobe using multilayer mirrors. *Nucl. Instrum. Meth. A* **266,** 296–303 (1988).
63. Buonassisi, T. *et al.* Synchrotron-based investigations of the nature and impact of iron contamination in multicrystalline silicon solar cells. *J. Appl. Phys.* **97,** 074901 (2005).
64. Buonassisi, T. *et al.* Engineering metal-impurity nanodefects for low-cost solar cells. *Nature Mater.* **4,** 676–679 (2005).
65. Liu, Y. *et al.* Applications of hard X-ray full-field transmission X-ray microscopy at SSRL. *Proc. 10th Int. Conf. X-ray Microscopy* (ed. McNulty, I.) (American Institute of Physics Conference Proceedings, in the press).
66. Gustafsson, M. G. L. Surpassing the lateral resolution limit by a factor of two using structured illumination microscopy. *J. Microsc.* **198,** 82–87 (2000).
67. Hell, S. W. & Kruog, M. Ground-state depletion fluorescence microscopy, a concept for breaking the diffraction resolution limit. *Appl. Phys. B* **60,** 495–497 (1995).
68. Beetz, T. & Jacobsen, C. Soft X-ray radiation damage studies in PMMA using a cryo-STXM. *J. Synchrotron Rad.* **10,** 280–283 (2003).
69. Weiss, D. *et al.* Computed tomography of cryogenic biological specimens based on X-ray microscopic images. *Ultramicroscopy* **84,** 185–197 (2000).
70. McDermott, G., Le Gros, M. A., Knoechel, C., Uchida, M. & Larabell, C. A. Soft X-ray tomography and cryogenic light microscopy: The cool combination in cellular imaging. *Trends Cell Biol.* **19,** 587–595 (2009).
71. Schneider, G. *et al.* 3D cellular ultrastructure resolved by a partially-coherent X-ray microscope. *Nat. Methods* (in the press).
72. Larabell, C. A. & Le Gros, M. A. X-ray tomography generates 3-D reconstructions of the yeast, *Saccharomyces cerevisiae*, at 60 nm resolution. *Mol. Biol. Cell* **15,** 957–962 (2004).
73. Le Gros, M. A., McDermott, G. & Larabell, C. A. X-ray tomography of whole cells. *Curr. Opin. Struc. Biol.* **15,** 593–600 (2005).
74. Meyer-Ilse, W. *et al.* High resolution protein localization using soft X-ray microscopy. *J. Microsc.* **201,** 395–403 (2001).
75. Stampanoni, M. *et al.* in *Advancements in Neurological Research* (ed. Zhang, J. H.) 315–335 (Research Signpost, 2008).
76. Brown, G. E. & Sturchio, N. C. An overview of synchrotron radiation applications to low temperature geochemistry and environmental science. *Rev. Mineral. Geochem.* **49,** 1–115 (2002).
77. Skinner, L. B., Chae, S. R., Benmore, C. J., Wenk, H. R. & Monteiro, P. J. M. Nanostructure of calcium silicate hydrates in cements. *Phys. Rev. Lett.* **104,** 195502 (2010).
78. Kurtis, K. E., Monteiro, P. J. M., Brown, J. T. & Meyer-Ilse, W. Imaging of ASR gel by soft X-ray microscopy. *Cement Concrete Res.* **28,** 411–421 (1998).
79. Monteiro, P. J. M. *et al.* Characterizing the nano and micro structure of concrete to improve its durability. *Cement Concrete Comp.* **31,** 577–584 (2009).
80. Kaulich, B. *et al.* Low-energy X-ray fluorescence microscopy opening new opportunities for bio-related research. *J. Res. Soc. Interface* **6,** 641–647 (2009).
81. Tolra, R. *et al.* Localization of aluminium in tea (*Camellia sinensis*) leaves using low energy X-ray fluorescence spectro-microscopy. *J. Plant Res.* doi:10.1007/s10265-010-0344-3 (2010).
82. Obst, M. *et al.* Precipitation of amorphous CaCO3 (aragonite-like) by cyanobacteria: A STXM study of the influence of EPS on the nucleation process. *Geochim. Cosmochim. Ac.* **73,** 4180–4198 (2009).
83. Obst, M., Wang, J. & Hitchcock, A. P. Soft X-ray spectro-tomography study of cyanobacterial biomineral nucleation. *Geobiology* **7,** 577–591 (2009).
84. Dynes, J. *et al.* Speciation and quantitative mapping of metal species in microbial biofilms using scanning transmission X-ray microscopy. *Environ. Sci. Technol.* **40,** 1556–1565 (2006).
85. Cotte, M. Synchrotron-based X-ray spectromicroscopy used for the study of an atypical micrometric pigment in 16th century paintings. *Anal. Chem.* **79,** 6988–6994 (2007).
86. Cotte, M., Susini, J., Dik, J. & Janssens, K. Synchrotron-based X-ray absorption spectroscopy for art conservation: looking back and looking forward. *Accounts Chem. Res.* **43,** 705–714 (2010).
87. Janssens, K., Dik, J., Cotte, M. & Susini, J. Photon-based techniques for nondestructive subsurface analysis of painted cultural heritage artifacts. *Accounts Chem. Res.* **43,** 814–825 (2010).
88. Lahlil, S., Biron, I., Cotte, M., Susini, J. & Menguy, N. Synthesis of calcium antimonite nano-crystals by the 18th dynasty Egyptian glassmakers. *Appl. Phys. A* **98,** 1–8 (2010).
89. Donaghue, P. *et al.* Synchrotron X-ray tomographic microscopy of fossil embryos. *Nature* **442,** 680–683 (2006).
90. Bergmann, U. *et al.* Archaeopteryx feathers and bone chemistry fully revealed via synchrotron imaging. *Proc. Natl Acad. Sci. USA* **107,** 9060–9065 (2010).
91. Bergmann, U. Archimedes brought to light. *Phys. World* 39–42 (November 2007).
92. Takman, P. A. C. *et al.* High-resolution compact X-ray microscopy. *J. Microsc.* **226,** 175–181 (2007).
93. Bertilson, M., von Hofsten, O., Vogt, U., Holmberg, A. & Hertz, H. M. High-resolution computed tomography with a compact soft X-ray microscope. *Opt. Express* **17,** 11057–11065 (2009).
94. Berglund, M., Rymell, L., Hertz, H. M. & Wilhein, T. Cryogenic liquid-jet target for debris-free laser-plasma soft X-ray generation. *Rev. Sci. Instrum.* **69,** 2362–2364 (1998).
95. Hemberg, O., Otendal, M. & Hertz, H. M. Liquid-metal-jet anode electron-impact X-ray source. *Appl. Phys. Lett.* **83,** 1483–1485 (2003).
96. Emma, P. *et al.* First lasing and operation of an angstrom-wavelength free-electron laser. *Nature Photon.* **4,** 641–647 (2010).
97. Parkinson, D. Y., McDermott, G., Etkin, L. D., Le Gros, M. A. & Larabell, C. A. Quantitative 3-D imaging of eukaryotic cells using soft X-ray tomography. *J. Struct. Biol.* **162,** 380–386 (2008).

Acknowledgements

The authors acknowledge support from the US National Science Foundation, the Engineering Research Center for EUV Science and Technology, and the King Abdullah University of Science and Technology.

Additional information

The authors declare no competing financial interests.